

# Peptides that block hepatitis B virus assembly: analysis by cryomicroscopy, mutagenesis and transfection

**B.Böttcher**<sup>1,2</sup>, **N.Tsuji**<sup>3</sup>, **H.Takahashi**<sup>3</sup>,  
**M.R.Dyson**<sup>4,5</sup>, **S.Zhao**<sup>4</sup>, **R.A.Crowther**<sup>1,6</sup> and  
**K.Murray**<sup>4,6</sup>

<sup>1</sup>Medical Research Council, Laboratory of Molecular Biology, Hills Road, Cambridge CB2 2QH, <sup>4</sup>Institute of Cell and Molecular Biology, University of Edinburgh, Edinburgh EH9 3JR, UK and <sup>3</sup>Gastrointestinal Unit, Harvard Medical School and Massachusetts General Hospital, Boston, MA 02114, USA

<sup>2</sup>Present address: Institut für Physikalische Chemie, Universität Freiburg, Albertstrasse 23a, D-79104 Freiburg, Germany

<sup>5</sup>Present address: Peptide Therapeutics, 321 Cambridge Science Park, Milton Road, Cambridge CB4 4WG, UK

<sup>6</sup>Corresponding authors

B.Böttcher and N.Tsuji contributed equally to this work

**Peptides selected to bind to hepatitis B virus (HBV) core protein block interaction with the long viral surface antigen (L-HBsAg) *in vitro*. High resolution electron cryomicroscopy showed that one such peptide binds at the tips of the spikes of the core protein shell. The peptides contain two basic residues; changing either of two acidic residues at the spike tip to an alanine greatly reduced the binding affinity. Transfection of hepatoma cells with a replication-competent HBV plasmid gave significantly reduced production of virus in the presence of peptide, in a dose-dependent manner. These experiments show that the interaction of L-HBsAg with core particles is critical for HBV assembly, and give proof of principle for its disruption *in vivo* by small molecules.**

**Keywords:** difference imaging/electron cryomicroscopy/hepatitis B virus/peptide inhibitors/virus assembly

## Introduction

Hepatitis B virus (HBV) consists of an inner nucleocapsid, comprising the core protein (HBcAg), viral polymerase and viral DNA, surrounded by a membranous envelope containing viral surface antigens (HBsAg). There are three surface antigen proteins [long (L), medium (M) and short (S)], which share a common C-terminal region but have different N-termini, arising from variable use of different initiation triplets within a continuous open reading frame. The L-polypeptide consists of preS1, preS2 and S regions, whereas the M-polypeptide consists of preS2 and S regions. The S region is believed to be predominantly membrane-bound while the preS regions, which are important for both viral assembly and attachment to the host cell during infection, are exposed to the cytosol on the endoplasmic reticulum when newly synthesized. However, in some molecules the preS region is translocated across the lipid bilayer and exposed on the virus surface (Neurath *et al.*, 1986; Bruss and Ganem, 1991; Ueda

*et al.*, 1991; Bruss *et al.*, 1994). Specific interactions between the outer surface of the core and the inner surface of the envelope are likely to guide correct assembly of the virus and stabilize the resulting particle. Earlier work has shown that L-HBsAg binds to the core protein *in vitro* (Dyson and Murray, 1995). Furthermore, using phage display libraries, peptides were selected which themselves bound to the core protein and blocked the binding of L-HBsAg to the core protein (Dyson and Murray, 1995). Such peptides are not found as a continuous sequence within the L-HBsAg polypeptide but represent mimics of the site of interaction with the core protein.

The core protein can be expressed efficiently in *Escherichia coli* (Pasek *et al.*, 1979), where it assembles into icosahedral shells of two sizes containing either 180 (T = 3) or 240 (T = 4) subunits (Crowther *et al.*, 1994). The subunits are clustered as dimers and each dimer forms a spike which protrudes on the surface of the shell. Using electron cryomicroscopy and image processing, a map of the T = 4 shell was recently made at 7.4 Å resolution from images of >6000 individual particles (Böttcher *et al.*, 1997). This revealed the fold of the polypeptide chain, which was largely  $\alpha$ -helical and quite unlike previously solved viral capsids. Each dimer spike was formed by a pair of long  $\alpha$ -helical hairpins, one from each monomer in the dimer (Böttcher *et al.*, 1997; Conway *et al.*, 1997). A numbering scheme which superimposed the amino acid sequence on the fold (Böttcher *et al.*, 1997) placed the major immunodominant region of the core protein, at approximately amino acids 78–82 (Salfeld *et al.*, 1989; Sällberg *et al.*, 1991), at the tip of the spike.

The methods used to determine the fold of the core protein have here been applied to locate, by cryomicroscopy, the binding sites on the core protein of one of the peptides that inhibits binding to L-HBsAg. This approach has now shown the peptide bound to the tips of the spikes, in both T = 3 and T = 4 shells. There are two acidic residues (Glu77 and Asp78) close to the tip of the core protein, and the selected binding peptides contain two conserved basic residues. The importance of these oppositely charged residues in the binding reaction was confirmed when mutation of either of the acidic residues in the protein to alanine was found to greatly reduce the affinity of the peptides for the altered core shells.

The inhibitory effect of the peptides on the interaction between core and surface proteins in infected cells was examined through transfection of permeabilized hepatoma Hep G2 cells with a replication-competent plasmid carrying a head-to-tail dimer of the HBV genome in the presence or absence of the peptide. In the presence of the peptide, production of virus particles was significantly reduced, providing proof of principle for the concept of using small molecules to bind to subunit interfaces and thus interfere with viral assembly.

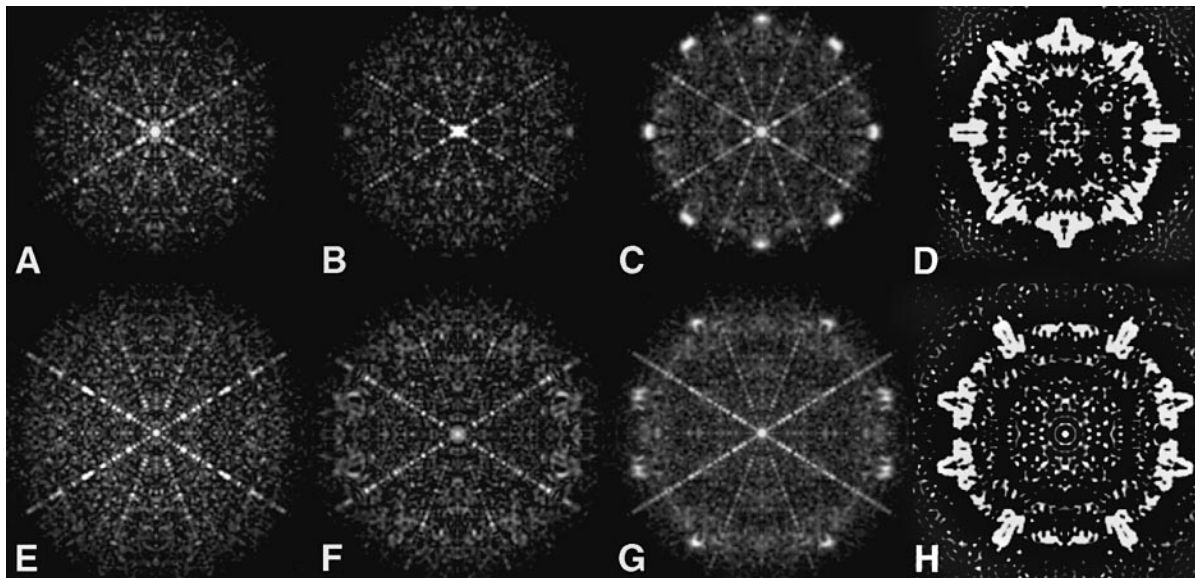


**Fig. 1.** Equatorial sections of standard deviation and density maps. (A–D) are from the  $T = 3$  shells and (E–H) are from the  $T = 4$  shells. The standard deviation maps in (A), (B), (E) and (F) were each calculated from five independent density maps. The maps in (A) and (E) show the standard deviation for the native structures, and (B) and (F) for structures plus peptide. (C) and (G) show the standard deviation for the combined data set of native and native plus peptide (10 maps). (A), (B), (E) and (F) show only the lines of the symmetry axes against a general background, whereas (C) and (G) have a set of strong peaks at positions corresponding to the tips of the spikes (see text). The sections in (D) and (H) are from density maps of native structures and show the positions of the spikes in the  $T = 3$  and  $T = 4$  shells. All plots are at the same magnification, such that the edge of subpanel (H) corresponds to  $\sim 400$  Å.

## Results

### **Location of the peptide-binding site on the core protein**

Peptides used in these studies are based on those described previously (Dyson and Murray, 1995) and were synthesized following random mutagenesis of residues flanking the peptide LLGRMK in the fusion phage B1 and reselection against HBcAg in a bio-panning reaction to obtain derivatives that bind the antigen with improved affinity. For structural investigations, a peptide (GSSLGRMKGA) with high affinity for HBcAg was bound to shells consisting of full-length core protein. The micrographs indicated that the population of particles contained  $\sim 60\%$  of  $T = 3$  and  $40\%$  of  $T = 4$  shells. Four three-dimensional maps were computed from native  $T = 3$  and  $T = 4$  shells with and without bound peptide. Fourier shell correlations indicated that all four maps were reliable to spacings of at least  $8.5$  Å (see Materials and methods) and so the final maps were all truncated at this point to ensure comparability.

Because the expected differences in density arising from peptide binding were small, standard deviation maps were calculated, first for the native shell, then for the shell plus peptide and finally for native and native plus peptide data combined. In the standard deviation maps from the single data sets, the positions of the icosahedral symmetry axes stand out as lines of density against a general low level noise speckle (Figure 1A, B, E and F). This is the behaviour expected, since noise on the symmetry axes does not cancel out as effectively as does noise at general points during the icosahedral averaging processes used in computing the map. In the standard deviation maps for the combined data sets, an additional set of strong peaks is seen for both  $T = 3$  and  $T = 4$  shells (Figure 1C and G). These strong peaks, which lie at positions corresponding to

the tips of the spikes of the core protein, indicate the regions of greatest difference between the native and the native plus peptide maps. The equatorial sections shown each pass through eight spikes. In the  $T = 3$  shell, these correspond to the dimers on strict and local 2-fold axes (Figure 1D), whereas in the  $T = 4$  shell all peaks are on local 2-fold axes (Figure 1H). The dimer spikes are cut at different angles, which accounts for the different appearances of the peaks in the standard deviation maps, but each section has *mm* symmetry arising from the orthogonal 2-fold axes in the section.

Having established objectively from the standard deviation maps the limited extent of the regions of principal difference between the native and native plus peptide maps, the density corresponding to the bound peptide could be visualized in difference maps (Figure 2). For both shells, we show the native map, the native plus peptide map and the difference map superimposed on the native map. In each case, to aid comparison, we focus on a ring of six dimers. For the  $T = 3$  shell, these lie around a strict 3-fold axis, with strict and local dimers alternating (Figure 2A–C). For the  $T = 4$  shell, they lie around a strict 2-fold axis and comprise the two computationally independent local dimers (four of one kind and two of the other) (Figure 2D–F). At the tip of each dimer, the difference density lies over the cleft between the two  $\alpha$ -helical hairpins and spills a short way down the side of the dimer spike. The difference densities in the  $T = 4$  map are less well defined, probably because fewer particles were included. The position of the difference density, lying across the local 2-fold axes, suggests that only a single copy of the peptide could be bound at any given tip, in one of two possible orientations, a situation similar to that reported for binding of an Fab antibody fragment to the spike tip (Conway *et al.*, 1998).

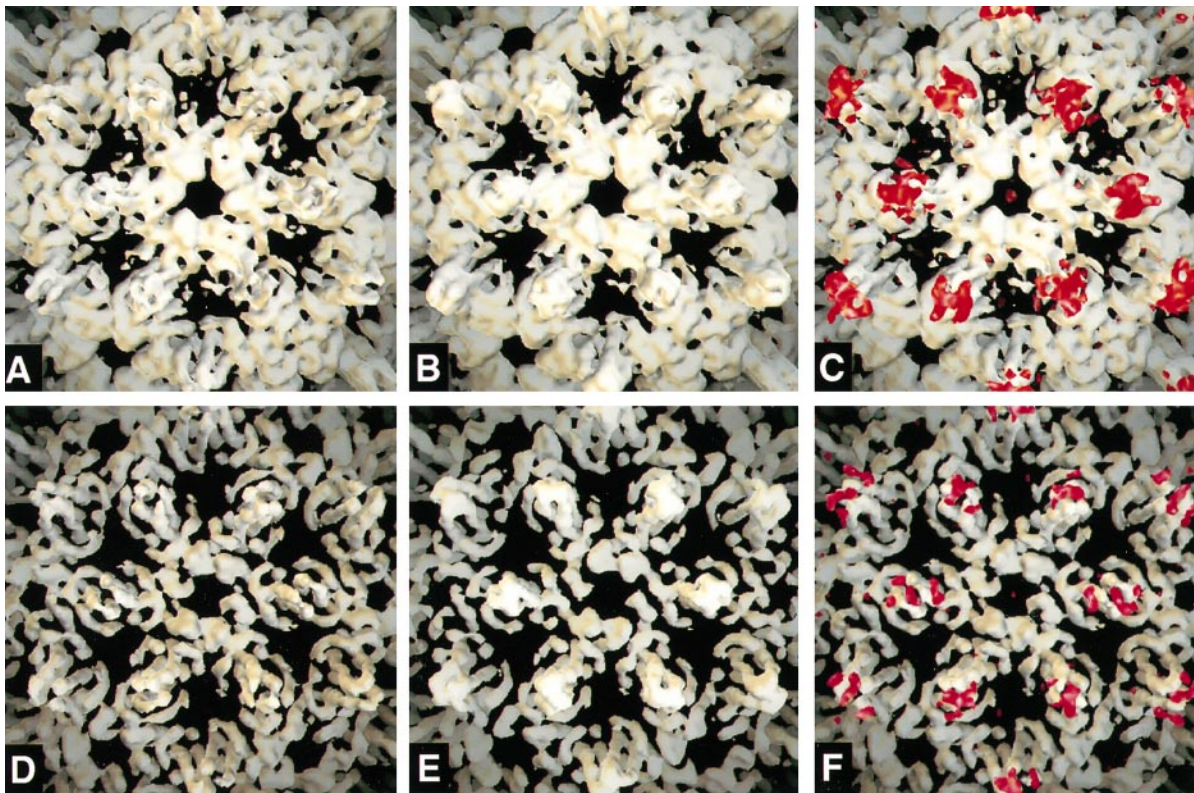


**Fig. 2.** Surface representations of  $T = 3$  and  $T = 4$  maps, showing part of the shell viewed down a local 6-fold axis. (A–C) show the  $T = 3$  map (strict 3-fold view) and (D–F) show the  $T = 4$  map (strict 2-fold view) of shells built from the full-length protein. (A) and (D) represent the native shell, whereas (B) and (E) show the shells with the peptide GSSLGRMKGA added. In (C) and (F), the difference map between native plus peptide minus native [(B) – (A) or (E) – (D)] is superimposed in red on the native map. The differences are concentrated at the tips of the spikes. The edge length of each panel corresponds to  $\sim 185$  Å.

#### Chemical cross-linking of peptide to HBcAg

The peptide MHRSSLGRMKGA, which has an enhanced affinity for HBcAg, was cross-linked to the antigen particles using 1-ethyl-3-(3-dimethylaminopropyl) carbodiimide hydrochloride (EDC) and *N*-hydroxysulfosuccinimide (sulfo-NHS). These reagents link adjacent primary amino and carboxyl groups to form an amide bond (Staros *et al.*, 1986). When added to the peptide–HBcAg complex, they should covalently cross-link the lysine from the peptide to a neighbouring aspartate or glutamate from HBcAg, causing its molecular weight to increase. Figure 3 shows a band shift corresponding to  $\sim 1$  kDa occurring on SDS–PAGE for a fraction of the HBcAg, when EDC and sulfo-NHS were added to the peptide–HBcAg complex. Despite trying the reaction under various conditions, no yield of  $>50\%$  of the shifted protein band was obtained. This is consistent with one peptide binding to a dimer of HBcAg close to the local 2-fold axis and thus sterically blocking binding of another peptide to the 2-fold related site, in agreement with the interpretation of the maps from electron cryomicroscopy.

#### Mutation of core protein residues important for peptide binding

The peptides selected by binding fusion phage to the core protein all contain two basic residues separated by a hydrophobic residue. This suggests that acidic residues on the core protein may provide at least part of the binding site for peptides. Our image analysis shows that the peptide-binding sites lie at the tip of the spikes which in

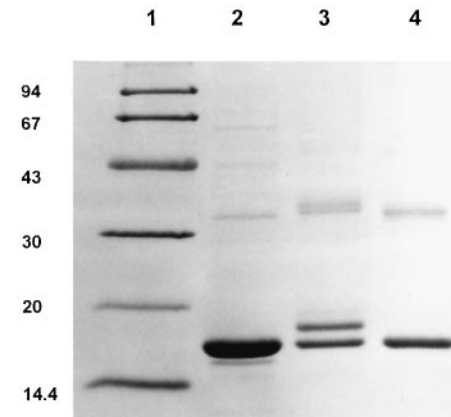


**Fig. 3.** Gel showing chemical cross-linking results. Lane 1, size markers (numbers on the left are relative molecular masses in kDa); lane 2, HBcAg alone; lane 3, HBcAg plus the peptide MHRSSLGRMKGA and cross-linker; lane 4, HBcAg plus cross-linker. In lane 3,  $\sim 50\%$  of the core protein shows a retarded mobility equivalent to  $\sim 1$  kDa.

the proposed numbering scheme for the polypeptide fold (Böttcher *et al.*, 1997) corresponds to residues in the region of amino acids 78–82, and there is a glutamic acid at 77 and an aspartic acid at 78. Accordingly, each of these residues was mutated in turn to an alanine. The relative dissociation constants ( $K_d^{\text{rel}}$ ) for reactions in solution between fusion phage 2A-8 carrying the peptide RSSLGRMK and the wild-type and mutant core proteins were measured as described previously (Dyson *et al.*,

1995). The results shown in Figure 4 indicate  $K_d$  values of 0.6 nM for wild-type, 100 nM for the D78A mutant, and 640 nM for the E77A mutant. Thus, changing Asp78 to alanine reduces the affinity 160-fold and changing Glu77 to alanine reduces the affinity 1000-fold, indicating that either or both acidic residues are important in binding the peptide.

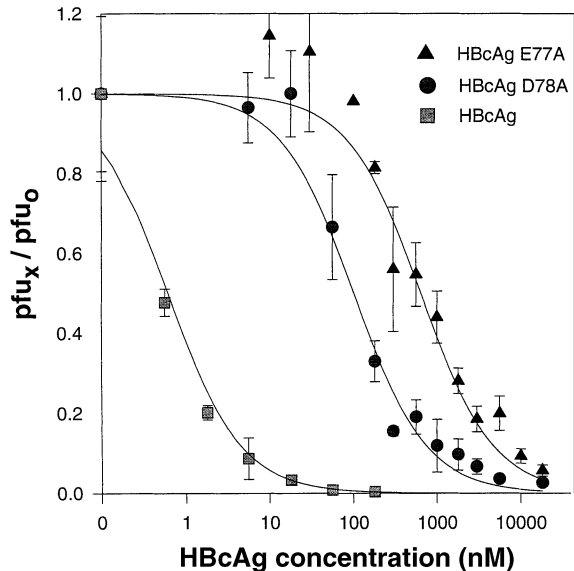


**Fig. 4.** Measurement of the relative dissociation constant for fusion phage 2A-8 binding to native and mutant core protein. A competition assay was used in which fusion phages (carrying the peptide RSLGRMK) were incubated with different concentrations of native or mutant core protein. The fraction of phage still available to bind to native core protein adsorbed on a solid surface was then measured. The number of recovered phage ( $pfu_x$ ) is represented as a fraction of the number of input phage ( $pfu_0$ ). The  $K_d$  values for the native protein and the mutants D78A and E77A were 0.6, 100 and 640 nM, respectively (see text).

### Peptide reduces virus yield from transfected cells

In order to see whether inhibitory peptides could interfere with virus production *in vivo*, human hepatoblastoma Hep G2 cells were transfected with a replication-competent plasmid carrying a head-to-tail dimer of the HBV genome (pHBV-HTD; Takahashi *et al.*, 1995) in the presence or absence of peptide. For quantification of the production of HBV in the culture supernatant, a radioactive PCR method was used after DNase digestion and immunoprecipitation of HBV particles with a monoclonal antibody specific for HBsAg (see Materials and methods). The method was validated by applying it to a serially diluted virus preparation. Figure 5A and B shows a linear relationship ( $R = 1.000$ ) between incorporation of  $^{33}P$ -labelled dCTP into the PCR product and the copy number of control HBV linearized 3.2 k bp DNA fragments, and provided a standard curve (Figure 5B) for calculation of HBV DNA copy number in the transfection experiments.

Inhibition of HBV production by three peptides exhibiting different affinities for HBcAg was compared in Hep G2 human hepatoblastoma cell lines transfected with pHBV-HTD. The plasmid DNA and the peptide were introduced simultaneously into cells that had been treated with TRANS PORT, a transient cell permeabilization reagent, and HBV production was measured after incubation of the cultures for 72 h. The peptide ALLTRILG, includes amino acids 21–27 of the S region of HBsAg. It shows a highly significant sequence match of five residues with the inhibitory peptide first identified, i.e. ALLGRMKG, but had no inhibitory effect on the interaction between HBcAg and L-HBsAg (Dyson and Murray, 1995); it also had no influence on HBV production in the transfection experiments and was therefore used as a control for non-specific effects of the addition of the peptides.

The reduced yields of virus in the presence of the three peptides relative to that with the control peptide are shown

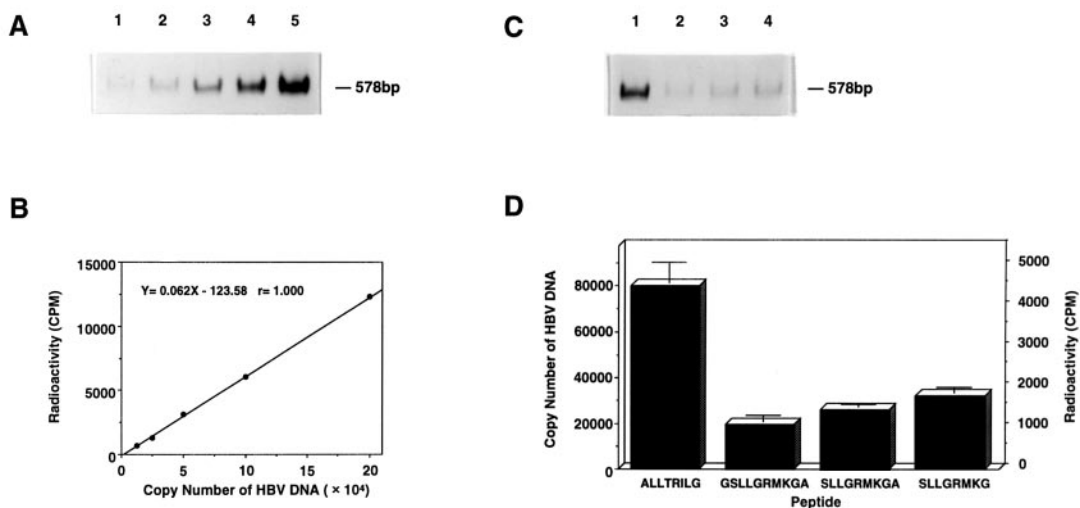


**Fig. 5.** Production of HBV by transfected cells in the presence of various inhibitory peptides. (A and B) Calibration of quantitative radioactive PCR for measuring viral copy number showing (A) gel electrophoresis of PCR products from serial 2-fold dilutions of an HBV preparation and (B) a plot of radioactivity against viral copy number. Note the extremely good linear relationship. (C and D) Virus production in the presence of different peptides, showing (C) radioautographs of PCR products separated by gel electrophoresis and (D) a histogram of radioactivity and corresponding viral copy number. The gel tracks (C) and histogram columns (D) correspond to peptides as follows: 1, ALLTRILG; 2, GSLGRMKGA; 3, SLLGRMKGA; 4, SLLGRMKG. The control peptide (1) does not bind to HBcAg, whereas peptides 2–4 bind to HBcAg with different affinities, the respective  $IC_{50}$  values for inhibition of L-HBsAg binding being 0.8, 2.4 and 6.4  $\mu M$ .

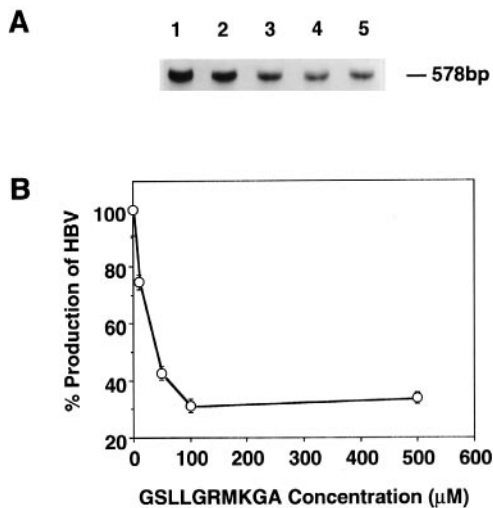


**Fig. 6.** Inhibition of virus production as a function of inhibitory peptide concentration. (A) Radioautographs of PCR products obtained from experiments at various peptide concentrations and separated by gel electrophoresis. (B) Yield of PCR product bands relative to that in the absence of peptide [lane 1 in (A)].

in Figure 5C and D, and the relative inhibitory effects of the three peptides reflect their affinities for HBcAg. To confirm that inhibition of HBV production in the presence of the peptides did not result from impaired growth of the transfected cells, their viability was assessed with a quantitative colorimetric dye reduction assay (Mosmann, 1983) on the cultures after 72 h. This showed no difference between cells transfected in the presence or absence of the peptides (results not shown). Inhibition of the association between HBcAg and L-HBsAg by the peptides is concentration dependent. Figure 6 shows that this is also the case for inhibition of HBV production in the hepatoma cells transfected in the presence of the peptide GSSLGRMKGA in the concentration range of 1–100 μM, above which the effect plateaued.

## Discussion

Chronic infection and antigenic variation mean that in spite of efficient vaccines against pathogenic agents, there will be a continuing need for therapeutic agents (compounds that impair or prevent production of the pathogens). The control of tuberculosis, at least temporarily, in many parts of the world emphasizes the critical importance of multiple drug therapy in containing the emergence of resistant strains of any pathogen, be it microbial or viral (Ryan, 1992). Nucleoside analogues and other small molecules that inhibit replication of viral genomes have been used to control viraemia, and peptides that match parts of viral coat or nucleocapsid protein sequences have been shown to reduce viral yield with influenza (Collier *et al.*, 1991) and with Sindbis and vesicular stomatitis viruses (Collier *et al.*, 1992). Similarly, small (non-peptide) molecules that bind to protein subunits of capsids have been shown to impair the assembly of procapsids in the *Salmonella typhimurium* phage P22, in which mechanisms of viral assembly can be studied conveniently *in vitro* (Teschke *et al.*, 1993), and Block *et al.* (1998) have shown very recently that inhibition of protein folding by blocking glycosylation can reduce viral

load in woodchucks chronically infected with HBV. The experiments described here show that peptide ligands identified by selection from essentially random populations of sequences in fusion phage display libraries, and which are mimics of a reaction interface rather than a replica of a part of a continuous protein sequence, may serve a similar function.

Differential analysis of large numbers of electron cryomicroscopy images of HBV nucleocapsid shells generated in the presence or absence of a given oligopeptide show the position at which the peptide is bound. This was amongst the smallest differences currently detected by electron cryomicroscopy and image processing. The method thus provides a powerful and fast tool for locating small peptides bound to the nucleocapsid shells, without the necessity for additional gold labelling, which carries the risk of disturbing the binding of the peptides. The resolution achieved was such that the residues likely to be involved in binding the peptide could be indicated and then confirmed by chemical cross-linking and site-directed mutagenesis of candidate amino acids in the HBcAg subunits. There is no conventional laboratory animal that can be infected with human HBV. The various members of the *hepadnaviridae* show a high species specificity, and human HBV will normally infect only a limited number of higher primates, but the virus can be produced (but not propagated) in cultured hepatoma cells by transfection. The peptides used in the electron cryomicroscopy and chemical cross-linking studies and others carrying the LLGRMK sequence reduced the yield of HBV in transfected hepatoma cell cultures in a dose-dependent manner and with relative efficiencies that reflect the  $IC_{50}$  values for the peptides in reactions between HBcAg and L-HBsAg in solution.

The observed impact on viral yield by peptides that block the interaction between L-HBsAg and HBcAg is consistent with the proposed role of the PreS1 domain in assembly of virus particles (Ueda *et al.*, 1991) and with the demonstration by Bruss *et al.* (1994) that the PreS1 region of newly synthesized L-HBsAg is cytosol-oriented to facilitate virus assembly. This proof of principle illustrates the value of combining a selection of ligands from an essentially random phage display library with high resolution structural analysis to map binding sites of primary lead compounds for development of small non-peptide molecules that inhibit biologically important reactions, such as those involved in virus assembly, and which in turn may be useful for extending the range of therapeutic agents.

## Materials and methods

### HBcAg preparations

Expression of either HBcAg (amino acids 3–183) or C-terminally truncated HBcAg (amino acids 3–148) in *E. coli* and purification were performed as described previously (Dyson and Murray, 1995). Protein preparations were stored at 4°C as sucrose gradient fractions in a buffer containing Tris-buffered saline (TBS), sucrose (20%) and  $NaN_3$  (0.02%). Preparations were stable in this form for at least 6 months.

### Chemical cross-linking of peptide to HBcAg

Truncated HBcAg (15 μg) was incubated at room temperature in a buffer (30 μl) containing potassium phosphate (25 mM, pH 7), NaCl (150 mM), EDC (1.8 mM) and sulfo-NHS (1.8 mM) in the presence or absence of the peptide MHRSLGRMKGA (1 mM). After 18 h, the

reaction was analysed by SDS-PAGE (15% w/v) as described (Sambrook *et al.*, 1989). EDC and sulfo-NHS were from Pierce Europe B.V. (The Netherlands), and the peptide was obtained from Albachem, University of Edinburgh, UK.

#### Mutagenesis of HBcAg and fusion phage binding assay

A *Bam*HI-*Eco*RI DNA fragment from plasmid pRI-11E (Stewart, 1993; Dyson and Murray, 1995) encoding amino acids 3–148 of HBcAg was ligated to the M13mp18 vector DNA (Sambrook *et al.*, 1989) and used to transform *E. coli* CJ236 for production of the uracil-containing single-stranded template DNA. Site-directed mutagenesis (Kunkel, 1985) was performed using the primers 5'-CTGGATCTGCTAAATTAG-3' and 5'-ATGCTGGAGCTTCTAAAT-3' to introduce the E77A and D78A mutations, respectively. The *Bam*HI-*Eco*RI fragment from the mutated DNA was then ligated to the *Bam*HI-*Eco*RI-digested pRI-11E vector for protein expression, and mutant HBcAg was purified as described above. The assay to determine the relative dissociation constants between the HBcAg preparations and fusion phage was as described (Dyson *et al.*, 1995) except that fusion phage 2A-8, bearing the sequence RSLGRMK, was employed. This fusion phage, having a higher affinity for HBcAg, was isolated by affinity purification from a sub-library of fd fusion phage B1 (carrying the sequence LLGRMK, Dyson and Murray, 1995), which was generated by insertion of random hexanucleotide sequences immediately before the codons for the LLGRMK sequence that had been inserted into gpIII in this phage.

#### Transfection experiments

Human hepatoblastoma cells, Hep G2 (American Type Culture Collection, Rockville, MD) were cultured in the presence of CO<sub>2</sub> (5%) at 37°C in Dulbecco's modified Eagle's medium (DMEM; BioWhittaker Inc., Walkersville, MD) supplemented with fetal bovine serum [FBS, 10% (v/v); Sigma Chemical Co., St Louis, MO] that had been incubated at 56°C for 30 min and supplemented with non-essential amino acids (100 µM), penicillin (100 U/ml) and streptomycin (100 µg/ml). Transfections were performed on low-passage cells with a transient cell permeabilization kit, TRANS PORT (Gibco-BRL, Grand Island, NY), according to the manufacturer's instructions; 5 × 10<sup>5</sup> cells were suspended in the intracellular buffer (290 µl) containing the TRANS PORT reagent and pHBV-HTD DNA (10 µg; Takahashi *et al.*, 1995) and incubated at 37°C for 10 min. The stop solution provided in the kit was then added and the cells incubated in DMEM supplemented with 10% (v/v) FBS at 37°C for a recovery period of 3 h. The peptides (kindly given by J.H.Cuervo, Biogen Inc. or obtained from Albachem, University of Edinburgh, UK) (100 µM; see Figure 6) were added to the cells at the beginning of the permeabilization and recovery stages. The extent of permeabilization was monitored by staining with trypan blue; ~70% of the cells became blue 10 min after treatment with TRANS PORT, and 64% of these cells lost the dye during the recovery period. Cell viability was assessed by means of a dye reduction assay (Mosmann, 1983) with 3-(4,5-dimethylthiazol-2-yl)-2,5-diphenyl tetrazolium bromide (MTT); cell suspensions (200 µl) were incubated in 96-well culture plates (Falcon 3072 Microtest III Tissue culture plate, Becton Dickinson, Lincoln Park, NJ) at 37°C for 72 h, and MTT solution (2.5 mg/ml in H<sub>2</sub>O; 10 µl) was added and the cells incubated at 37°C for a further 4 h. The culture plates were centrifuged (500 g; 5 min) and the culture supernatants removed and mixed with 0.04 M HCl in iso-propanol (100 µl) to dissolve the blue formazan product; after 5 min at room temperature, the absorbance at 590 nm of the solutions was measured with a microculture plate reader (Microplate Reader, Model 7520, Cambridge Technology Inc., Watertown, MA).

#### Measurement of HBV production

Cell culture supernatants (200 µl) were treated with DNase (Sigma Chemical Co., St Louis, MO; 20 U/ml) at 37°C for 15 min to degrade any plasmid or free HBV DNA. EDTA (0.5 M, pH 8.0, 10 µl) was then added and virus particles were absorbed with the murine anti-HBsAg monoclonal antibody, 5D3, conjugated to azolactone-acrylamide copolymer beads (3M Emphaze™ Biosupport Medium, A.B.I., Pierce, Rockford, IL) (Takahashi *et al.*, 1988, 1995). After extensive washing, HBV DNA was released from the beads by heating at 95°C for 10 min and quantified by means of PCR with [ $\alpha$ -<sup>33</sup>P]dCTP (DuPont NEN Research Products, Boston, MA) and primers to yield a 578 bp fragment from the HBcAg reading frame (sense primer, 5'-GAGAATTCAGCCT-CCAAGCTGTGCCTTGG-3'; antisense primer, 5'-GAAAGCTTCTG-CGACGCGCGATTGAGA-3'). The PCR was carried out in a mixture (50 µl) containing the DNA sample (20 µl), MgCl<sub>2</sub> (2.5 mM), the two primers (1 µM each), dNTPs (0.01 mM), *Taq* DNA polymerase (Ampli-

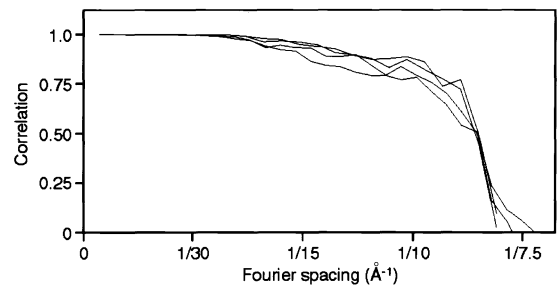


**Fig. 7.** Fourier shell correlations for the different reconstructions. For all four reconstructions, the Fourier shell correlation drops to 0.5 at ~8.3 Å.

*Taq* Gold, Perkin Elmer, Foster City, CA; 1.25 U) and [ $\alpha$ -<sup>33</sup>P]dCTP (10 µCi) with amplification cycles of 95°C for 30 s, 50°C for 1 min and 72°C for 3 min. After 30 cycles, the products were separated by electrophoresis in 6% (w/v) polyacrylamide gels; product bands were located by radioautography, excised, and the radioactivity measured with a liquid scintillation spectrometer (Beckman Instruments, Fullerton, CA). For quantification in terms of HBV, a standard curve was constructed from PCRs with known quantities of linearized HBV DNA (3.2 kb). As a control to ensure the absence of the transfecting plasmid in the immunoprecipitated samples, PCRs were carried out with the sense primer 5'-CTGCAAGCCGATTAAGTTGGGTAA-3' (for the *lacZ* sequence of the plasmid) substituted for the sense primer for the HBcAg sequence; these yield a 2524 bp product, identified by electrophoresis in a 1.5% (w/v) agarose gel after 35 PCR cycles of 95°C for 30s, 50°C for 1 min and 72°C for 1 min.

#### Electron microscopy

Grids coated with perforated carbon film were glow discharged in air four times for 15 s. Air was let in between each discharge. These grids were then used within 1 h. A 2 µl aliquot of core protein sample (10 mg/ml) or core protein sample (6–10 mg/ml) mixed with the peptide GSELLGRMKGA (1 mg/ml) was applied to a grid mounted in a modified controlled environment freezing apparatus (Bellare *et al.*, 1988) and then frozen in liquid ethane.

For electron microscopy, grids were mounted in a Gatan cold stage and then transferred to a Hitachi FE 2000 electron microscope equipped with a field emission gun. The microscope was operated under low dose conditions and micrographs were taken at a nominal magnification of 60 000 and a dose between 1500 and 2000 e/nm<sup>2</sup> on Kodak SO163 film.

#### Image processing

Micrographs were scanned with a Zeiss SCAI-scanner with a step size of 14 µm per pixel corresponding to 2.3 Å on the specimen. Magnification of the microscope was calibrated previously using tobacco mosaic virus (Böttcher and Crowther, 1996). Three-dimensional maps were computed for T = 3 shells (5424 particles in the absence of peptide and 5010 particles in the presence of bound peptide) and T = 4 shells (3319 particles in the absence of peptide and 3612 particles in the presence of bound peptide). T = 4 particles were aligned to a 7.4 Å resolution map of T = 4 hepatitis B core protein shells (Böttcher *et al.*, 1997) using cross common lines (Crowther *et al.*, 1994). Then the current best map was used for further refinement of the following components: defocus for each micrograph, scaling of each particle, particle origin (x and y) and particle orientation ( $\theta$ ,  $\phi$  and  $\omega$ ). From each micrograph, an independent map was calculated. The maps were combined and corrected for the contrast transfer function (Böttcher and Crowther, 1996). The T = 3 particles were processed similarly. They were aligned initially to a 30 Å resolution map of T = 3 hepatitis B core protein shells (Crowther *et al.*, 1994) and then refined further against the current best model.

The resolution of the maps was assessed by dividing the data in half, calculating two independent maps and then calculating the Fourier shell correlation (Figure 7). For all four reconstructions, the correlation drops to 0.5 at ~8.3 Å. The final maps were truncated at Fourier spacings above 8.5 Å and below 200 Å, and an inverse temperature factor of 540 Å<sup>2</sup> was applied. The maps were scaled in their grey values by multiplying with a constant factor to give about the same lowest and highest grey values, and then one map was subtracted from the other. For calculating standard deviation maps of a single reconstruction, data were divided into five parts. Care was taken that a good spread of defocus values was included in each individual map. Independent maps

were computed and then the standard deviation between the five maps calculated. For comparing maps with and without peptide, the standard deviation of all 10 maps (five with peptide bound and five without) was calculated.

## Acknowledgements

B.B. was supported by an EC Human Capital and Mobility Grant. The work was supported in part by Biogen Inc., Cambridge MA., and by grant No. NIDDK 4331 from the National Institutes of Health (USA).

## References

- Bellare, J.R., Davis, H.T., Scriven, L.E. and Talmon, Y. (1988) Controlled environment vitrification system: an improved sample preparation technique. *J. Electron Microsc. Tech.*, **10**, 87–111.
- Block, T.M. *et al.* (1998) Treatment of chronic hepatitis B infection in a woodchuck animal model with an inhibitor of protein folding and trafficking. *Nature Med.*, **4**, 610–614.
- Böttcher, B. and Crowther, R.A. (1996) Difference imaging reveals ordered regions of RNA in turnip yellow mosaic virus. *Structure*, **4**, 387–394.
- Böttcher, B., Wynne, S.A. and Crowther, R.A. (1997) Determination of the fold of the core protein of hepatitis B virus by electron cryomicroscopy. *Nature*, **386**, 88–91.
- Bruss, V. and Ganem, D. (1991) The role of envelope protein in hepatitis B virus assembly. *Proc. Natl Acad. Sci. USA*, **88**, 1059–1063.
- Bruss, V., Lu, X., Thomssen, R. and Gerlich, W.H. (1994) Post-translational alteration in transmembrane topology of hepatitis B virus large envelope protein. *EMBO J.*, **13**, 2273–2279.
- Collier, N.C., Knox, K. and Schlesinger, M.J. (1991) Inhibition of influenza virus formation by a peptide that corresponds to sequences in the cytoplasmic domain of the hemagglutinin. *Virology*, **183**, 769–772.
- Collier, N.C., Adams, S.P., Weingarten, H. and Schlesinger, M.J. (1992) Inhibition of enveloped RNA virus formation by peptides corresponding to glycoprotein sequences. *Antiviral Chem. Chemother.*, **3**, 31–36.
- Conway, J.F., Cheng, N., Zlotnick, A., Wingfield, P.T., Stahl, S.J. and Steven, A.C. (1997) Visualization of a 4-helix bundle in the hepatitis B virus capsid by cryo-electron microscopy. *Nature*, **386**, 91–94.
- Conway, J.F., Cheng, N., Zlotnick, A., Stahl, S.J., Wingfield, P.T., Belnap, D.M., Kanngiesser, U., Noah, M. and Steven, A.C. (1998) Hepatitis B virus capsid: localization of the putative immunodominant loop (residues 78 to 83) on the capsid surface and implications for the distinction between c and e-antigens. *J. Mol. Biol.*, **279**, 1111–1121.
- Crowther, R.A., Kiselev, N.A., Böttcher, B., Berriman, J.A., Borisova, G.P., Ose, V. and Pumpens, P. (1994) Three-dimensional structure of hepatitis B virus core particles determined by electron microscopy. *Cell*, **77**, 943–950.
- Dyson, M.R. and Murray, K. (1995) Selection of peptide inhibitors of interactions involved in complex protein assemblies: association of the core and surface antigens of hepatitis B virus. *Proc. Natl Acad. Sci. USA*, **92**, 2194–2198.
- Dyson, M.R., Gernaschewski, V. and Murray, K. (1995) Direct measurement via phage titre of the dissociation constants in solution of fusion phage–substrate complexes. *Nucleic Acids Res.*, **23**, 1531–1535.
- Kunkel, T.A. (1985) Rapid and efficient site-specific mutagenesis without phenotypic selection. *Proc. Natl Acad. Sci. USA*, **82**, 488–492.
- Mosmann, T. (1983) Rapid colorimetric assay for cellular growth and survival: application of proliferation and cytotoxicity assays. *J. Immunol. Methods*, **65**, 55–63.
- Neurath, A.R., Kent, S.B.H., Strick, N. and Parker, K. (1986) Identification and chemical synthesis of a host cell receptor binding site on hepatitis B virus. *Cell*, **46**, 429–436.
- Pasek, M., Goto, T., Gilbert, W., Zink, B., Schaller, H., MacKay, P., Leadbetter, G. and Murray, K. (1979) Hepatitis B virus genes and their expression in *E. coli*. *Nature*, **282**, 575–579.
- Ryan, F. (1992) *Tuberculosis: The Greatest Story Never Told*. Swift Publishers, Bromsgrove, UK.
- Salfeld, J., Pfaff, E., Noah, M. and Schaller, H. (1989) Antigenic determinants and functional domains in core antigen and e antigen from hepatitis B virus. *J. Virol.*, **63**, 798–808.
- Sällberg, M., Ruden, U. and Magnius, L.O. (1991) Characterisation of a linear binding site for a monoclonal antibody to hepatitis B core antigen. *J. Med. Virol.*, **33**, 248–252.
- Sambrook, J., Fritsch, E.F. and Maniatis, T. (1989) *Molecular Cloning: A Laboratory Manual*. 2nd edn. Cold Spring Harbor Laboratory Press, Cold Spring Harbor, NY.
- Smith, G.P. and Scott, J.K. (1993) Libraries of peptides and proteins displayed on filamentous phage. *Methods Enzymol.*, **217**, 228–257.
- Staros, J.V., Wright, R.W. and Swingle, D.M. (1986) Enhancement by *N*-hydroxysulfosuccinimide of water-soluble carbodiimide-mediated coupling reactions. *Anal. Biochem.*, **156**, 220–222.
- Stewart, F.J. (1993) Mutations that affect the structure and interactions of the core antigen of hepatitis B virus. PhD thesis, University of Edinburgh, Scotland.
- Takahashi, H., Kameda, H. and Wands, J.R. (1988) Development of a second generation monoclonal immunoradiometric assay. Increased sensitivity leads to enhanced detection of hepatitis B viral infection. *J. Immunol. Methods*, **112**, 191–200.
- Takahashi, H., Fujimoto, J., Hanada, S. and Isselbacher, K.J. (1995) Acute hepatitis in rats expressing human hepatitis B virus transgenes. *Proc. Natl Acad. Sci. USA*, **92**, 1470–1474.
- Teschke, C.M., King, J. and Prevelige, P.E. (1993) Inhibition of viral capsid assembly by 1,1'-bi (4-anilinoanthracene)-5-sulfonic acid. *Biochemistry*, **32**, 10658–10665.
- Ueda, K., Tsurimoto, K. and Matsubara, K. (1991) Three envelope proteins of hepatitis B virus: large S, middle S and major S proteins needed for the formation of Dane particles. *J. Virol.*, **65**, 3521–3529.

Received July 22, 1998; revised and accepted September 25, 1998